Thermodynamic integration by neural network potentials based on first-principles dynamic calculations

Shogo Fukushima, Eisaku Ushijima, Hiroyuki Kumazoe, Akihide Koura, and Fuyuki Shimojo
Department of Physics, Kumamoto University, Kumamoto 860–8555, Japan

Kohei Shimamura
Graduate School of System Informatics, Kobe University, Kobe 657–8501, Japan

Masaaki Misawa
Faculty of Science and Engineering, Kyushu Sangyo University, Fukuoka 813–8503, Japan

Rajiv K. Kalia, Aiichiro Nakano ⬤, and Priya Vashishta
Collaboratory for Advanced Computing and Simulations, University of Southern California, Los Angeles, California 90089, USA

Simulation-size effect in evaluating the melting temperature of material is studied systematically by combining thermodynamic integration (TI) based on first-principles molecular-dynamics (FPMD) simulations and machine learning. Since the numerical integration to determine the free energies of two different phases as a function of temperature is very time consuming, the FPMD-based TI method has only been applied to small systems, i.e., less than 100 atoms. To accelerate the numerical integration, we here construct an interatomic potential based on the artificial neural-network (ANN) method, which retains the first-principles accuracy at a significantly lower computational cost. The free energies of the solid and liquid phases of rubidium are accurately obtained by the ANN potential, where its weight parameters are optimized to reproduce FPMD results. The ANN results reveal a significant size dependence up to 500 atoms.

I. INTRODUCTION

Phase transition plays an important role in a wide range of scientific and engineering problems [1]. To accurately calculate the phase-transition temperature, the thermodynamic integration (TI) method has been used by calculating the free energies of two different phases [2–15]. Frenkel and Ladd used the TI method to calculate the free energies of solid phases by Monte Carlo simulation [2]. Sugino and Car pioneered the TI method based on first-principles molecular-dynamics (FPMD) simulations to study the solid-liquid phase transition of Si, using density functional theory (DFT) within the local density approximation [3]. Wang *et al.* calculated the Gibbs free energies of solid and liquid carbon by the FPMD-based TI method under pressure [8]. Their melting curve is in good agreement with the experimental triple point and is consistent with shockwave experiments. More recently, Taniguchi and Tsuchiya obtained the melting curve of MgO under high pressure by the first-principles TI method [14]. They discussed thermodynamic phase stability under the Jovian core conditions. The TI method has also been used to estimate the melting temperature of other materials such as Al [4,5], Fe [6,15], Si [7], C [9], Mo [10], Xe [11], ZrC [12], and Cu [13]. While the FPMD-based TI method can obtain the transition temperature with sufficient precision, its high computational cost severely limits the system size that can be studied. Although it has been claimed that less than 100 atoms are sufficient with multiple k-point sampling for Si [3,7], size

dependence of the calculated transition temperature has not been quantified systematically. Therefore, it is important to investigate the dependence of the calculated free energy on the system size.

In order to handle adequate system sizes while retaining first-principles accuracy, we here adopt an interatomic potential constructed by artificial neural-network (ANN) models trained by FPMD simulations [16–20]. In previous studies, ANN potentials were constructed for several materials, including Na [17], ZnO [18], and H_2O [19]. It is conceivable that the computational cost of numerical integration in the TI method is greatly reduced by using an ANN potential compared with FPMD-based TI calculations, while keeping first-principles accuracy. It then becomes possible to obtain the free energy of sufficiently large systems. Recently, Grabowski *et al.* have applied a machine-learning technique to TI calculations using moment tensor potentials (MTPs) as an intermediate reference to obtain vibrational free energies of alloys [21], by extending a similar technique [12,13] but using empirical potentials such as embedded atom method (EAM). They showed that the MTP free energy is only 1 meV/atom away from the DFT free energy. In this paper, we demonstrate that the ANN-based TI method gives the free energy within the accuracy of less than 0.1 meV/atom in the case of rubidium with more than 100 atoms.

It is well known that a maximum exists in the pressure-dependent melting temperature T_m of alkali metals [22–25]. Raty *et al.* studied the electronic and structural transitions

of liquid Na under pressure of up to 120 GPa using FPMD simulations [24]. They reported that the T_m of Na drops from 1000 K at 30 GPa to room temperature at 120 GPa with increasing pressure. Yamane *et al.* also performed FPMD simulations to investigate the melting curve of Na as a function of pressure by taking into account the effects of semicore $2p$ electrons [25]. They showed that the maximum T_m is 900–1000 K at pressures of 20–30 GPa when only $3s$ electrons are considered, while it is 1000–1100 K at 40–80 GPa when treating both $2p$ and $3s$ electrons as the valence states. These theoretical studies determined the pressure dependence of T_m by directly observing the melting and crystallization phenomena in FPMD simulations at a given pressure or volume, which commonly exhibits large hysteresis to make the determination of the transition temperature difficult. To precisely determine the melting curve of alkali metals under pressure, it is necessary to evaluate the phase-transition temperature with high precision instead using the TI method. This study aims to (1) show that the free energy obtained by the ANN potential is in good agreement with that obtained by the FPMD method, and (2) use the former to determine the dependence of the transition temperature on the system size.

II. COMPUTATIONAL METHODS

A. Thermodynamic integration

The difference between the Helmholtz free energies of two different systems can be evaluated by the TI method. If a system with analytically known free energy is used as a reference system, the absolute value of the Helmholtz free energy of the target system can be obtained. Following previous studies using the TI method [14], we use an Einstein solid (ES) and an ideal gas (IG) as reference systems of the solid and liquid phases, respectively. These reference systems have been used not only for transition temperatures but also for the formation energy of atomic vacancies [26] and the solubility of materials into liquid [27].

When the interaction energy U of a system depends on a parameter λ, we obtain the following formula:

$$\frac{\partial F(\lambda)}{\partial \lambda} = \left\langle \frac{\partial U(\lambda)}{\partial \lambda} \right\rangle_{NVT}, \qquad (1)$$

where $F(\lambda)$ is the Helmholtz free energy and $\langle \cdots \rangle_{NVT}$ denotes the canonical (NVT) ensemble average. The interaction energy $U(\lambda)$ is given by

$$U(\lambda) = \lambda U_{Rb} + (1 - \lambda) U_{ref} \quad (0 \leqslant \lambda \leqslant 1), \qquad (2)$$

where U_{Rb} and U_{ref} are the potential energies of the target (Rb) and reference systems, respectively. By integrating both sides of Eq. (1) with respect to λ from 0–1, we obtain

$$F(\lambda = 1) - F(\lambda = 0) = \int_0^1 \langle U_{Rb} - U_{ref} \rangle_{NVT} d\lambda, \qquad (3)$$

where $F(\lambda = 1)$ and $F(\lambda = 0)$ are the free energies of the target and reference systems, respectively.

The free energy is obtained by numerically integrating the right-hand side of Eq. (3) using the molecular-dynamics (MD) method in the canonical ensemble. To ensure that the canonical ensemble is accurately generated, an independent
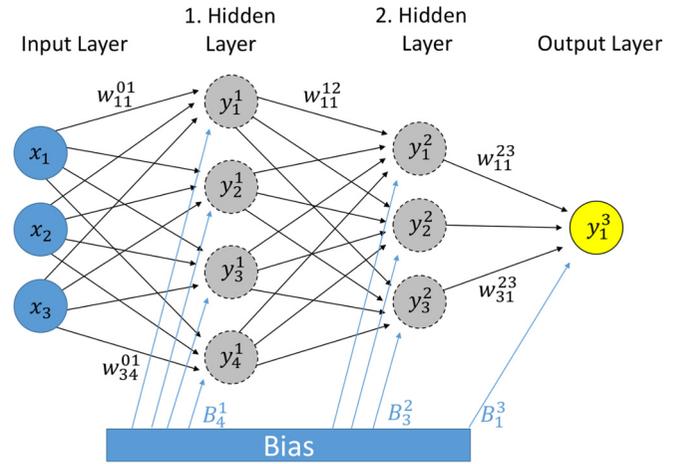

FIG. 1. Structure of a simple feed-forward neural network (FFNN). The value in the output layer (yellow) is obtained as a function of the input values x in the input layer (cyan). There are several hidden layers comprised of nodes. The black arrows represent the weight parameters $\omega_{i,\,j}^{k,\,l}$. The bias weights B_j^l (cyan arrows) are used as adjustable parameters to shift the activation function.

Nosé-Hoover chain is attached to each degree of freedom of the system involving the ES [26], because a harmonic oscillator does not exhibit an ergodic behavior. On the other hand, the standard Nosé-Hoover thermostat for the entire system is used for the liquid state.

B. Artificial neural network (ANN)

Accurate numerical integration in Eq. (3) requires a prohibitively large number of MD steps, for which we use an interatomic potential constructed by the ANN method [16]. ANN is a collection of connected nodes called artificial neurons, which are inspired by biological neurons in brain. The coupling strength between the artificial neurons can be changed by training, with which ANN has an ability to approximate any function.

The feed-forward neural network (FFNN) is the simplest type of ANN [28,29], where only forward propagation of information from input nodes to output nodes is allowed. It has been applied to MD simulations for more than a decade [30–32]. Figure 1 shows the structure of a simple FFNN comprising an input layer, one or more hidden layers, and an output layer. The nodes of each layer are connected to the nodes in the adjacent layers by weight parameters, which are determined by fitting FPMD results. The value y_j^l of node j in layer l is given by

$$y_j^l = f_j^l \left(B_j^l + \sum_i \omega_{i,\,j}^{k,\,l} \cdot y_i^k \right), \qquad (4)$$

where $\omega_{i,\,j}^{k,\,l}$ is the weight parameter from node i in layer k to node j ($= i + 1$) in layer l ($= k + 1$), y_i^k is the input value from the previous layer k, and B_j^l is the bias weight, which is used as an adjustable parameter to shift the activation function f_j^l. The activation function used in this study is given by [33]

$$f^l(x) = a \tanh(bx) + cx, \qquad (5)$$

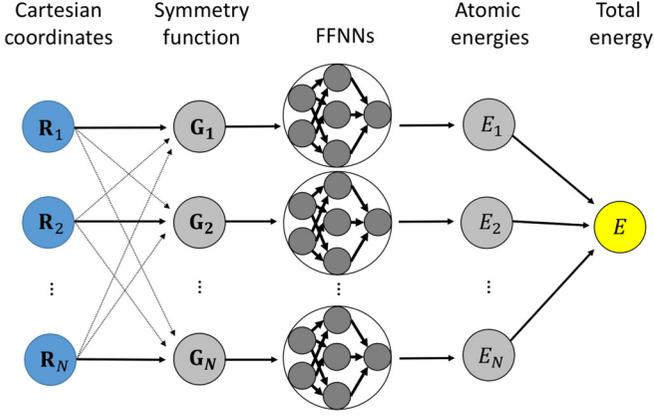where $a = 1.7195$, $b = 2/3$ and $c = 0.1$.

FIG. 2. Schematic of ANN potential construction [16]. The Cartesian coordinates $\{\mathbf{R}_i\}$ (cyan) are transformed into a set of symmetry function values $\mathbf{G}_i$ associated with each atom. These values depend on the position of all atoms in the system indicated by the gray arrows. The $\mathbf{G}_i$ values are used as the input values for the FFNNs and the atomic energies E_i are obtained as the output values. The total energy E (yellow) is obtained by summing E_i.

C. Symmetry functions

The total energy E is a sum of atomic energies [16],

$$E = \sum_i E_i, \tag{6}$$

where E_i is the energy associated with the ith atom. Figure 2 shows a schematic of ANN-potential construction. First, the Cartesian coordinates $\{\mathbf{R}_i\}$, which are obtained by first-principles calculations, are transformed into a set of symmetry function values $\mathbf{G}_i$ associated with each atom. These values depend on the positions of all atoms in the system. Next, the $\mathbf{G}_i$ values are used as the input values x for the FFNN (Fig. 1), and the atomic energies E_i are obtained as the output values. Finally, the total energy E is obtained by summing up E_i.

Symmetry functions were introduced in Ref. [34] and have been used for the construction of various ANN potentials [35,36] and other machine-learning tasks [37]. We use two types of symmetry functions: a radial function G_i^{rad} and an angular function G_i^{ang}. The radial function G_i^{rad} is given by

$$G_i^{\mathrm{rad}} = \sum_j e^{-\eta(R_{ij}-R_s)^2} \cdot f_c(R_{ij}), \tag{7}$$

where $R_{ij} = |\vec{R}_{ij}|$ is the distance between the ith and jth atoms, η and R_s are adjustable parameters, and $f_c(R_{ij})$ is a cutoff function defined as

$$f_c(R_{ij}) = \begin{cases} 0.5\left[\cos\left(\frac{\pi R_{ij}}{R_c}\right) + 1\right] & (R_{ij} \leqslant R_c) \\ 0 & (R_{ij} \geqslant R_c), \end{cases} \tag{8}$$

where R_c is the cutoff distance. The angular function G_i^{ang} is expressed as

$$G_i^{\mathrm{ang}} = 2^{1-\zeta} \sum_{j,k \neq i}^{\mathrm{all}} (1 + \lambda\cos\theta_{ijk})^\zeta \cdot e^{-\eta(R_{ij}^2 + R_{ik}^2 + R_{jk}^2)}$$
$$\cdot f_c(R_{ij}) \cdot f_c(R_{ik}) \cdot f_c(R_{jk}), \tag{9}$$

TABLE I. Parameter of the radial function G_i^{rad} of Eq. (7).

No.	η (Å^{-2})	R_s	No.	η (Å^{-2})	R_s
1	0.003	0.0000	9	0.070	4.0000
2	0.030	0.0000	10	0.120	4.0000
3	0.070	0.0000	11	0.200	4.0000
4	0.120	0.0000	12	0.070	5.0000
5	0.200	0.0000	13	0.120	5.0000
6	0.070	3.0000	14	0.200	5.0000
7	0.120	3.0000	15	0.070	6.0000
8	0.200	3.0000	16	0.120	6.0000
			17	0.200	6.0000

where θ_{ijk} is the angle between $\vec{R}_{ij}$ and $\vec{R}_{ik}$ with λ, ζ, and η being adjustable parameters.

Tables I and II list the parameters of the symmetry functions used in this study. The cutoff distance R_c is set to 10.5 Å. To construct ANN potentials based on the results of FPMD simulations, we use the atomic energy network (AENET) package [33,38].

D. FPMD simulations

FPMD simulations are carried out using a highly parallelized plane-wave DFT program [39], which calculates electronic states using the projector-augmented-wave (PAW) method [40,41]. The generalized gradient approximation (GGA) is used for the exchange-correlation energy [42]. The plane-wave cutoff energies are 8.0 and 60.0 Ry for the electronic pseudowave functions and pseudocharge density, respectively. The projector functions are generated for the $5s$ state of Rb. Three systems containing 54, 128, and 432 Rb atoms in a cubic supercell are used under periodic boundary conditions. Isothermal-isobaric (NPT) ensemble is employed for all FPMD simulations. The pressure is set to the ambient pressure. The equations of motion are solved via an explicit reversible integrator [43] with a time step of $\Delta t = 2.88$ fs. The Gaussian broadening [44] is used for the occupation numbers

TABLE II. Parameter of the angular function G_i^{ang} of Eq. (9).

No.	η (Å^{-2})	λ	ζ	No.	η (Å^{-2})	λ	ζ
18	0.0003	-1.0	1.0	33	0.0003	1.0	2.0
19	0.0100	-1.0	1.0	34	0.0100	1.0	2.0
20	0.0300	-1.0	1.0	35	0.0300	1.0	2.0
21	0.0500	-1.0	1.0	36	0.0500	1.0	2.0
22	0.0900	-1.0	1.0	37	0.0900	1.0	2.0
23	0.0003	1.0	1.0	38	0.0003	-1.0	2.0
24	0.0100	1.0	1.0	39	0.0100	-1.0	4.0
25	0.0300	1.0	1.0	40	0.0300	-1.0	4.0
26	0.0500	1.0	1.0	41	0.0500	-1.0	4.0
27	0.0900	1.0	1.0	42	0.0900	-1.0	4.0
28	0.0003	-1.0	2.0	43	0.0003	1.0	4.0
29	0.0100	-1.0	2.0	44	0.0100	1.0	4.0
30	0.0300	-1.0	2.0	45	0.0300	1.0	4.0
31	0.0500	-1.0	2.0	46	0.0500	1.0	4.0
32	0.0900	-1.0	2.0	47	0.0900	1.0	4.0
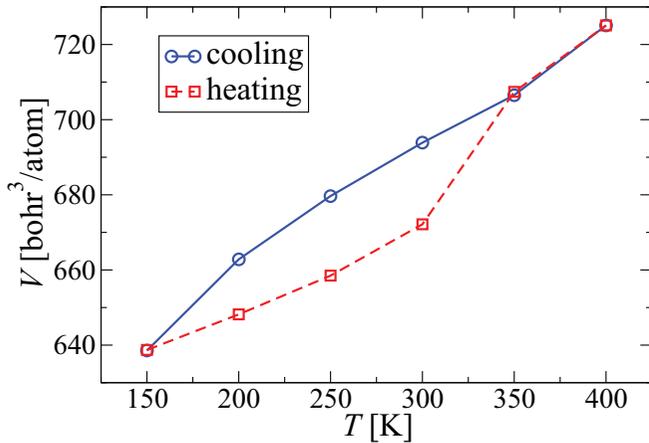
FIG. 3. Temperature dependence of the volume of the 128-atom system.

TABLE III. Root-mean-square errors (RMSEs) of the energies obtained by the ANN potentials for the training and test sets.

		RMSE [meV/atom]			
		Solid		Liquid	
No. of atoms	T [K]	Training set	Test set	Training set	Test set
54	220	0.0140	0.0155	0.0069	0.0072
	240	0.0267	0.0287	0.0078	0.0079
128	200	0.0086	0.0086	0.0055	0.0059
	250	0.0178	0.0184	0.0092	0.0095
	300	0.0082	0.0083	0.0047	0.0051
250	250	0.0023	0.0025	0.0022	0.0025
	300	0.0023	0.0030	0.0024	0.0025
432	250	0.0015	0.0017	0.0015	0.0017
	300	0.0016	0.0017	0.0016	0.0018

of one-electron KS states with a broadening parameter of 0.2 eV. The effect of this smearing on the TI results is likely small, owing to the cancellation when subtracting free energies between the solid and liquid phases.

III. RESULTS AND DISCUSSION

A. Freezing-melting hysteresis

To obtain the temperatures at which melting and crystallization phenomena occur in the current model system for Rb, we begin with the 128-atom system in the bcc crystalline state. When the temperature is increased from 150 K in increments of 50 K every 87 ps (30000 steps), melting occurs at 350 K. When the temperature is decreased in the same cooling rate as heating, the system in the liquid state crystallizes at 150 K. Figure 3 shows the dependence of the volume on temperature. The temperature range of this freezing-melting hysteresis becomes smaller if longer FPMD simulations are carried out. However, it is not possible to determine the phase-transition temperature precisely in this way due to the long time to perform such simulations.

B. Construction of ANN potentials

We construct the ANN potentials using the numerical data from the FPMD simulations for the 54-, 128-, and 432-atom systems. For both the liquid and solid phases at different temperatures, the respective ANN potentials are obtained by fitting the FFNN weight parameters to model E_i in Eq. (6) to reproduce the energies of 5000 ∼ 20000 atomic configurations. We randomly choose 10% of the reference data as the test data (test set) to detect overfitting, i.e., determining whether the ANN potential fits the test set as well as the remaining 90% of the data (training set) used to construct the ANN potential. The Levenberg-Marquardt method [45–47] is used for the fitting algorithm, which is highly parallelized in the reference-data space and scales linearly with the number of reference structures. Table III shows the root-mean-square errors (RMSEs) of the energies obtained by the ANN potentials for the training and test sets. The results show that the RMSEs are at most 0.03 meV/atom, corresponding to a small

temperature of 0.3 K, even for the test set. Namely, the ANN potentials are constructed accurately enough to estimate the melting temperature.

In Fig. 4, the total energies predicted by the ANN potentials are compared with their corresponding FPMD reference energies for the training and test sets in the case of the solid phase at 250 K of the 128-atom system. The inset in Fig. 4 shows the difference between the two energies. The small ΔE value demonstrates that the ANN potentials reproduce the FPMD reference data very well.

To demonstrate the accuracy of the ANN potentials in MD simulations, we calculate the radial distribution function $g(r)$, as shown in Fig. 5, where the solid and dotted lines represent the results obtained by the FPMD simulations and the ANN potentials, respectively. The results show that, in the 54-, 128-, 250-, and 432-atom systems, the $g(r)$'s for both the solid and liquid phases obtained by the ANN potentials are in good agreement with those calculated from the FPMD simulations.
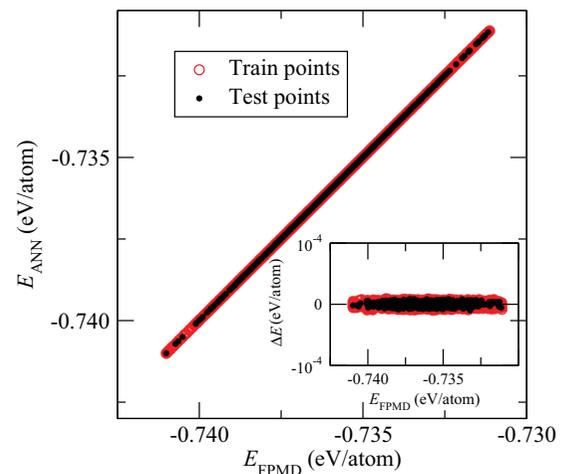

FIG. 4. Comparison of the ANN potential energies E_{ANN} and the corresponding FPMD reference energies E_{FPMD} for the training set (red open circles) and the test set (black dots) in the case of the solid phase at 250 K of the 128-atom system. The inset shows the difference, $\Delta E = E_{ANN} - E_{FPMD}$, as a function of E_{FPMD}.
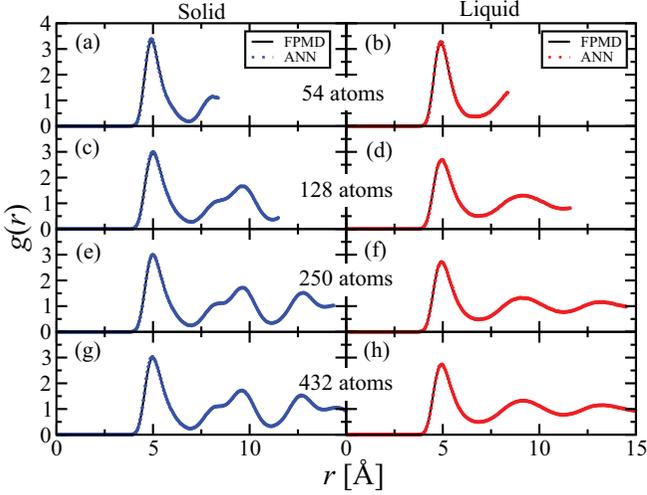
FIG. 5. Radial distribution functions $g(r)$ obtained for the solid (a) and liquid (b) phases at 220 K of the 54-atom system; solid (c) and liquid (d) phases at 250 K of the 128-atom system; solid (e) and liquid (f) phases at 250 K of the 250-atom system; and solid (g) and liquid (h) phases at 250 K of the 432-atom system. The solid and dotted lines represent the $g(r)$ calculated by FPMD simulations and ANN potentials, respectively. The $g(r)$'s obtained by the ANN potentials are in good agreement with those obtained by the FPMD simulations.

FIG. 6. λ dependence of (a) $\langle U_{\mathrm{Rb}} - U_{\mathrm{ES}} \rangle_{NVT}$ for the solid phase and (b) $\langle U_{\mathrm{Rb}} - U_{\mathrm{SC}} \rangle_{NVT}$ for the liquid phase at 220 K of the 54-atom system. The circles and crosses represent the results obtained by the FPMD simulations and the ANN potentials, respectively.

From these results, we expect that MD simulations using the ANN potentials have the same quality as the FPMD simulations regarding structural properties.

C. Thermodynamic integration (TI)

To confirm whether the ANN potentials can be applied to obtain the thermodynamic quantities, TI calculations are carried out for the solid and liquid phases at 220 K of the 54-atom system using the MD simulations based on the ANN potentials. The results are compared with those by the FPMD simulations. For the solid phase, the ES is used as the reference system. The potential energy U_{ES} is given by

$$U_{\mathrm{ES}}(\{\mathbf{r}_i\}) = \frac{1}{2} \sum_{i=1}^{N} m\omega^2 |\mathbf{r}_i - \mathbf{r}_{i0}|^2, \qquad (10)$$

where $\mathbf{r}_{i0}$ is the equilibrium position of the ith atom. The frequency $\omega = 7.4$ (ps^{-1}) is determined from the peak position of the Fourier transform of the velocity autocorrelation function of Rb atoms. To evaluate the Helmholtz free energy F_{Sol} of the solid phase, numerical integration of the right-hand side of Eq. (3) is performed by MD simulation for at least 58 ps (20000 steps) using 12 different λ values: 0, 0.3690, 0.6019, 0.7488, 0.8415, 0.9000, 0.9369, 0.9602, 0.9749, 0.9842, 0.9900, and 1. Figure 6(a) shows $\langle U_{\mathrm{Rb}} - U \rangle_{\mathrm{ES} NVT}$ as a function of λ, where the circles and crosses represent the results obtained by the FPMD simulations and the ANN potentials, respectively. It is seen that both results are in good agreement with each other. The difference between the Helmholtz free energies is only $\Delta F_{\mathrm{direct}} = -0.45 \, \mathrm{meV/atom}$, which is sufficiently small for the evaluation of the melting temperature T_{m} as discussed below. More precisely, the dif-
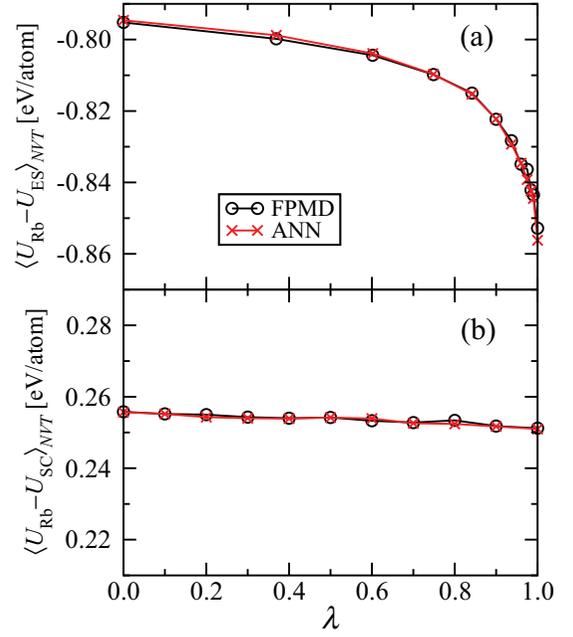
ference corresponds to the temperature of approximately 4 K; hence, we can discuss T_{m} within this accuracy.

For the liquid phase, the ideal gas is used as the reference system, whose potential energy U_{IG} is zero. The problem in numerically integrating the right-hand side of Eq. (3) for the liquid phase is that the distance between atoms becomes very small when λ approaches zero, which makes the electronic-structure calculations impossible to perform. To avoid short atomic distances in the FPMD simulations, we introduce a soft-core (SC) potential defined by

$$U_{\mathrm{SC}}(\{\mathbf{r}_i\}) = \sum_{i<j}^{N} \varepsilon \left(\frac{\sigma}{r_{ij}} \right)^n, \qquad (11)$$

where $\varepsilon = 5.0 \times 10^{-3}$ hartree, $\sigma = 8.0$ bohr, and $n = 12$, which are determined to make the first peak of $g(r)$ similar to that in the FPMD simulations. Therefore, the Helmholtz free energy F_{liq} of the liquid phase is obtained by two TIs: first from the ideal gas to the soft-core liquid, then from the soft-core liquid to the actual liquid. The former can be performed easily because the computational cost required for simulations of the soft-core liquid is very small. For the latter, we performed MD simulation for at least 58 ps (20000 steps) using 11 different λ values from zero to one with intervals of 0.1. As shown in Fig. 6(b), the λ dependence of $\langle U_{\mathrm{Rb}} - U_{\mathrm{SC}} \rangle_{NVT}$ calculated by the ANN potentials agrees very well with that obtained by the FPMD simulations. The difference between the Helmholtz free energies is only $\Delta F_{\mathrm{direct}} = 0.17 \, \mathrm{meV/atom}$, which is again sufficiently small.

The free energies reported in this paper were obtained using at least 20000 MD steps and more than 10 different λ values to achieve high numerical accuracies. Since these

TABLE IV. Free-energy difference, $\Delta F_{\text{TI}} = F_{\text{FPMD}} - F_{\text{ANN}}$, between TI calculations using DFT-based FPMD and ANN potential.

No. of atoms	T [K]	ΔF_{TI} [meV/atom]	
		Solid	Liquid
54	220	−0.42	0.17
128	250	−0.06	−0.02
250	250	−0.05	−0.03
432	250	−0.04	−0.04

computations using FPMD simulations are extremely time consuming for over 100 atoms, we have employed the ANN potentials instead to study the size effects on the melting temperature.

Reliability of the free energies thus calculated for more than 100 atoms was confirmed by estimating the free-energy difference, $\Delta F_{\text{TI}} = F_{\text{FPMD}} - F_{\text{ANN}}$, using TI calculations with DFT-based FPMD and ANN potential, as was done in Refs. [12,13,21]. For this purpose, much shorter MD runs and smaller number of λ values are expected to be sufficient, since $\Delta U = U_{\text{FPMD}} - U_{\text{ANN}}$ is very small as shown in Fig. 4. We found that 3000 MD steps and at most five different λ values are sufficient for TI within an error of less than 0.01 meV/atom. The results are shown in Table IV. For the 54-atom system, ΔF_{TI} values obtained for the solid and liquid states were consistent with ΔF_{direct} described above. It is seen that $|\Delta F_{\text{TI}}|$ of the systems with more than 100 atoms are less than 0.1 meV/atom, corresponding to a temperature within 1 K.

D. Size effects on melting temperature

As validated in the previous subsection, the TI method using ANN potentials is efficient and reliable. The ANN potentials constructed for the 54-, 128-, 250-, and 432-atom systems in Sec. III B are used in the TI method to obtain the Helmholtz free energy of the solid (F_{Sol}) and liquid (F_{liq}) phases of the respective systems. Figure 7 shows the free-energy difference ΔF ($= F_{\text{liq}} - F_{\text{Sol}}$) for the three systems as a function of temperature (solid symbols). From this figure, T_{m} is estimated to be 199 ± 4, 251 ± 4, 275 ± 4, and 283 ± 4 K for the 54-, 128-, 250-, and 432-atom systems, respectively, as shown in Fig. 8 (solid circles). Since T_{m} is systematically higher for larger systems, it is important to carefully consider the dependence of T_{m} on the system size. Using an asymptotic expansion of T_{m} up to the first-order term of $1/N$ to fit the data,

$$T_{\text{m}} = T_{\text{m}}^{\infty} - \frac{b}{N}, \tag{12}$$

we estimate the transition temperature of bulk Rb to be $T_{\text{m}}^{\infty} = 293 \pm 4$ K, which is comparable to the experimental value of 312 K [48]. The agreement is satisfactory considering that GGA was used in our FPMD simulations, and that the quantum corrections for the motion of atomic nuclei were not included. It has been shown that GGA provides lower melting temperatures than experiments [13], which is consistent with our results shown above.

The open circles in Fig. 7 show the ΔF obtained for the 432-atom system using the ANN potential constructed
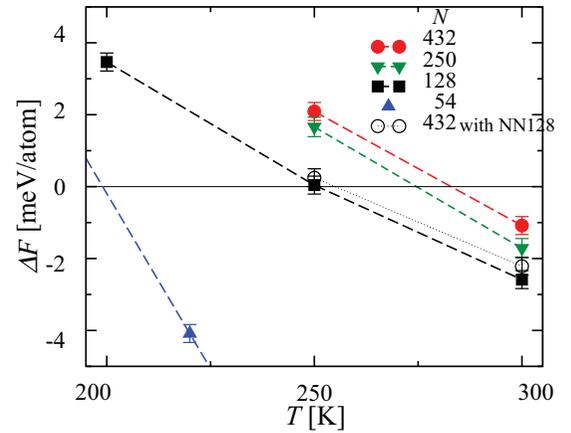

FIG. 7. Temperature dependence of ΔF ($= F_{\text{liq}} - F_{\text{Sol}}$). The solid up-pointing triangles, solid squares, solid down-pointing triangles, and solid circles represent the results for the 54-, 128-, 250-, and 432-atom systems, respectively, obtained by the ANN potentials constructed for the respective systems. The open circles represent the results for the 432-atom system using the ANN potential constructed with 128 atoms (NN128).

with 128 atoms. These values are not close to those for the 432-atom system (solid circles), but instead close to those for the 128-atom system (solid squares) using the ANN potential constructed with the same number of atoms. The T_{m} is estimated to be 255 ± 4 K as shown by the open circle in Fig. 8, which is almost the same as T_{m} for the 128-atom system, despite the result using 432 atoms. Further, T_{m} of a larger system containing 1,024 atoms was estimated using ANN potentials constructed with 128 and 432 atoms, as shown by black and red open diamonds, respectively, in Fig. 8. The two T_{m} values are close to those at which the respective ANN potentials are constructed (solid black square and solid red circle). These findings clearly indicate that it is important for the precise evaluation of T_{m} by the TI method to construct the ANN potential using the same number of atoms as that
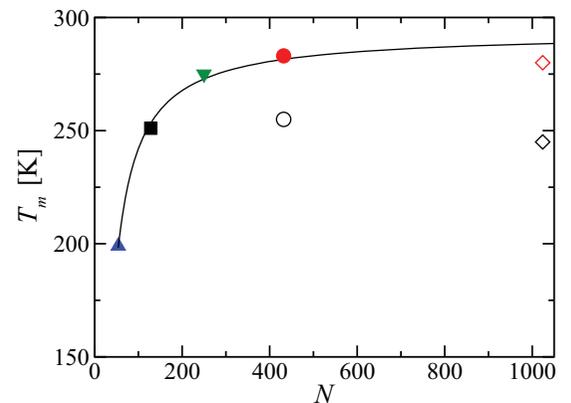

FIG. 8. Melting temperature T_{m} as a function of the number of atoms N. The symbols represent T_{m} values corresponding to those in Fig. 7. The black and red open diamonds represent the results for $N = 1024$ but using ANN potentials constructed with 128 and 432 atoms, respectively. The line represents the best fit, $T_{\text{m}} = a - b/N$, with $a = 293.4$ and $b = 5139$.

in a target system up to at least 432 atoms. Since the fitted weight parameters in an ANN potential learn the periodicity of the system used in the training, the results obtained by the ANN potential would reflect the same periodicity, irrespective of the size of system. The size dependence likely arises from spatially extended correlations in QMD simulations, which will be investigated in future work.

We have investigated the effects of semicore $4p$ electrons on the free energy for the 128-atom system. The difference between the free energies of solid and liquid phases calculated with and without $4p$ electrons are approximately 0.6 and 0.1 meV/atom, respectively, at 250 K. The results indicate that the melting temperature is affected only by several kelvins by the inclusion of $4p$ electrons.

Finally, we study the influence of k-point sampling in the Brillouin zone. We have calculated the free energy of the liquid state at 300 K for the 54-atoms system using $2 \times 2 \times 2$ k points, which corresponds to the system size of 432 atoms. The free energy decreases by 1.3 meV/atom, which is much smaller than the difference between the free energies of the 54- and 432-atom systems, 6.3 meV/atom, obtained by Γ point only. These results indicate that the accurate estimation of the melting temperature requires direct simulations of larger systems, and merely increasing the k points is not adequate for this purpose.

IV. CONCLUSION

We have demonstrated that the TI method using ANN potentials based on FPMD simulations is very efficient in obtaining the Helmholtz free energies of alkali metals with high accuracy and low computational cost. We have shown that the melting temperature becomes higher as the number of atoms in the system is increased, which suggests that size dependence should be carefully taken into account in TI calculations. Furthermore, we found that the estimated melting temperature of bulk material agrees well with the experimental value.

[1] R. E. Doe, K. A. Persson, Y. S. Meng, and G. Ceder, Chem. Mater **20**, 5274 (2008).

[2] D. Frenkel and A. J. C. Ladd, J. Chem. Phys. **81**, 3188 (1984).

[3] O. Sugino and R. Car, Phys. Rev. Lett. **74**, 1823 (1995).

[4] G. A. de Wijs, G. Kresse, and M. J. Gillan, Phys. Rev. B **57**, 8223 (1998).

[5] L. Vočadlo and D. Alfè, Phys. Rev. B **65**, 214105 (2002).

[6] D. Alfè, G. D. Price, and M. J. Gillan, Phys. Rev. B **65**, 165118 (2002).

[7] D. Alfè and M. J. Gillan, Phys. Rev. B **68**, 205212 (2003).

[8] X. Wang, S. Scandolo, and R. Car, Phys. Rev. Lett. **95**, 185701 (2005).

[9] F. Colonna, J. H. Los, A. Fasolino, and E. J. Meijer, Phys. Rev. B **80**, 134103 (2009).

[10] C. Cazorla, D. Alfè, and M. J. Gillan, Phys. Rev. B **85**, 064113 (2012).

[11] L. Shulenburger, M. P. Desjarlais, and T. R. Mattsson, Phys. Rev., B **90**, 140104(R) (2014).

[12] A. I. Duff, T. Davey, D. Korbmacher, A. Glensk, B. Grabowski, J. Neugebauer, and M. W. Finnis, Phys. Rev. B **91**, 214311 (2015).

[13] L.-F. Zhu, B. Grabowski, and J. Neugebauer, Phys. Rev. B **96**, 224202 (2017).

[14] T. Taniguchi and T. Tsuchiya, J. Phys. Condens. Matter **30**, 114003 (2018).

[15] T. Sun, J. P. Brodholt, Y. Li, and L. Vočadlo, Phys. Rev. B **98**, 224301 (2018).

[16] J. Behler and M. Parrinello, Phys. Rev. Lett. **98**, 146401 (2007).

[17] H. Eshet, R. Z. Khaliullin, T. D. Kühne, J. Behler, and M. Parrinello, Phys. Rev. B **81**, 184107 (2010).

[18] N. Artrith, T. Morawietz, and J. Behler, Phys. Rev. B **83**, 153101 (2011).

[19] T. Morawietz and J. Behler, J. Phys. Chem. A **117**, 7356 (2013).

[20] V. Botu and R. Ramprasad, Int. J. Quantum Chem. **115**, 1074 (2015).

[21] B. Grabowski, Y. Ikeda, P. Srinivasan, F. Körmann, C. Freysoldt, A. I. Duff, A. Shapeev, and J. Neugebauer, npj Comput. Mater. **5**, 80 (2019).

[22] C. L. Guillaume, E. Gregoryanz, O. Degtyareva, M. I. McMahon, M. Hanfland, S. Evans, M. Guthrie, S. V. Sinogeikin, and H-K. Mao, Nature Phys. **7**, 211 (2011).

[23] E. Gregoryanz, O. Degtyareva, M. Somayazulu, R. J. Hemley, and H. K. Mao, Phys. Rev. Lett. **94**, 185502 (2005).

[24] J. Y. Raty, E. Schwegler, and S. A. Bonev, Nature (London) **449**, 448 (2007).

[25] A. Yamane, F. Shimojo, and K. Hoshino, J. Phys. Soc. Jpn. **77**, 064603 (2008).

[26] E. Smargiassi and P. A. Madden, Phys. Rev. B **51**, 117 (1995).

[27] H. F. Wilson and B. Militzer, Phys. Rev. Lett. **108**, 111101 (2012).

[28] G. Cybenko, Math. Control Signals Syst. **2**, 303 (1989).

[29] K. Hornik, M. Stinchcombe, and H. White, Neural Netw. **2**, 359 (1989).

[30] C. M. Handley and P. L. A. Popelier, J. Phys. Chem. A **114**, 3371 (2010).

[31] S. Lorenz, A. Groß, and M. Scheffler, J. Chem. Phys. Lett. **395**, 210 (2004).

[32] S. Lorenz, M. Scheffler, and A. Gross, Phys. Rev. B **73**, 115431 (2006).

[33] N. Artrith and A. Urban, Comput. Mater. Sci. **114**, 135 (2016).

[34] J. Behler, J. Chem. Phys. **134**, 074106 (2011).

[35] G. C. Sosso, G. Miceli, S. Caravati, J. Behler, and M. Bernasconi, Phys. Rev. B **85**, 174103 (2012).

[36] N. Artrith and A. M. Kolpak, Comput. Mater. Sci. **110**, 20 (2015).

[37] E. D. Cubuk, S. S. Schoenholz, J. M. Rieser, B. D. Malone, J. Rottler, D. J. Durian, E. Kaxiras, and A. J. Liu, Phys. Rev. Lett. **114**, 108001 (2015).

[38] N. Artrith, A. Urban, and G. Ceder, Phys. Rev. B **96**, 014112 (2017).

[39] F. Shimojo, R. K. Kalia, A. Nakano, and P. Vashishta, Comput. Phys. Commun. **140**, 303 (2001).

[40] P. E. Blöchl, Phys. Rev. B **50**, 17953 (1994).

[41] G. Kresse and D. Joubert, Phys. Rev. B **59**, 1758 (1999).

[42] J. P. Perdew, K. Burke, and M. Ernzerhof, Phys. Rev. Lett. **77**, 3865 (1996).

[43] M. Tuckerman, B. J. Berne, and G. J. Martyna, J. Chem. Phys. **97**, 1990 (1992).

[44] C. Elsässer, M. Fähnle, C. T. Chan, and K. M. Ho, Phys. Rev. B **49**, 13975 (1994).

[45] K. Levenberg, Quart. Appl. Math. **2**, 164 (1944).

[46] D. W. Marquardt, J. Soc. Ind. Appl. Math. **11**, 431 (1963).

[47] M. Hagan and M. B. Menhaj, IEEE Trans. Neural Netw. **5**, 989 (1994).

[48] H. D. Luedemann and G. C. Kennedy, J. Geophys. Res. **73**, 2795 (1968).